Radio Science, Volume 34, Number 3, Pages 575–586, May–June 1999

Diffraction analysis of a double-shielded antenna in the Fraunhofer and Fresnel regimes: Model predictions

C. Tello,[1] T. Villela,[1] C. A. Wuensche,[1] N. Figueiredo,[2] S. Torres,[3,4] M. Bersanelli,[5] M. Bensadoun,[6] G. De Amici,[6,7] and G. F. Smoot [6]

Abstract. We analytically investigate the use of a wire mesh ground screen (fence) and a halo of extension panels around a helically fed parabolic reflector in order to estimate the ground contribution to the antenna noise temperature in an experiment aimed at surveying the sky at decimeter wavelengths. We use geometric diffraction theory to model the effect of these screening and blocking shields when scanning in azimuth at tilt angles from zenith in the range $0° \geq Z \geq 45°$. We report estimates based on existing formulas for monofilar axial-mode helical antennas with expected low-level sidelobes in the direction of the halo region. As long as there is no significant coupling between the near-field patterns of both the feed and the diffracting halo, estimates using the Fraunhofer approximation agree with those calculated with the Fresnel approach at a tilt angle Z_{eq}, which increases with the proximity of the diffracting edge from the near-/far-field boundary of the feed pattern. Our estimates show that for a fence of some 10-dB attenuation and high enough to level out the horizon profile at the prime focus of the antenna, the diffracted components dominate the contribution for tilt angles $Z \lesssim 35°$. The fence is the main diffractor when $Z \gtrsim 20°$, but for $Z \gtrsim 25°$ its contribution becomes insensitive to the presence of the halo. On the other hand, if the attenuation is low (<1 dB), the increase in ground solid angle with tilt angle makes the contribution due to transmission and ground exposure the dominant one.

[1]Instituto Nacional de Pesquisas Espaciais, São José dos Campos, São Paulo, Brazil.

[2]Escola Federal de Engenharia de Itajubá, Itajubá, Minas Gerais, Brazil.

[3]Observatorio Astronómico, Universidad Nacional de Colombia, Bogotá, Colombia.

[4]Also at Centro Internacional de Física, Bogotá, Colombia.

[5]Istituto di Fisica Cosmica, Consiglio Nazionale delle Ricerche, Milan, Italy.

[6]Lawrence Berkeley National Laboratory, Berkeley, California.

[7]Now at TRW, Redondo Beach, California.

Paper number 1998RS900031.
0048-6604/99/1998RS900031$11.00

1. Introduction

The remarkable progress of microwave astronomy and cosmology achieved in the last decade has brought renewed interest to producing reliable all-sky surveys of the galactic radio continuum [*De Amici et al.*, 1994; *Kogut et al.*, 1996a, b; *Davies et al.*, 1996]. In particular, the need to determine the precise level of contamination of the measurements of the cosmic microwave backgound radiation by diffuse foreground signals (galactic synchrotron, free-free, and dust components) led to the creation of the Galactic Emission Mapping (GEM) project [*De Amici et al.*, 1994], an international collaboration whose observational program is presently under way to produce all-sky maps of the total brightness

at 408 and 1465 MHz and 2.3, 5, and 10 GHz. The GEM experiment was conceived to overcome the base level and temperature scale uncertainties that plague existing surveys [*Haslam et al.*, 1982; *Reich and Reich*, 1986] in deriving the distribution of the synchrotron spectral index over the sky [*Lawson et al.*, 1987; *Reich and Reich*, 1988; *Platania et al.*, 1998]. Preliminary results of the collaboration have been presented in the form of partial sky maps by *Torres et al.* [1996] at 408 MHz, by *Tello* [1997] at 1465 MHz, and at 2.3 GHz by S. Torres (internal report, 1997).

One of the major causes for the striping seen in the preparation of previous maps is the varying level of sidelobe contribution due to transmitted and diffracted radiation from the ground. In this paper we model the novel approach introduced by the observational technique of the GEM project to minimize this effect at 408 and 1465 MHz. Our goal is to present an analytic description of the intended performance of the experiment. A forthcoming paper (C. Tello et al., manuscript in preparation, 1998) includes the measured response of the feeds to estimate the actual performance.

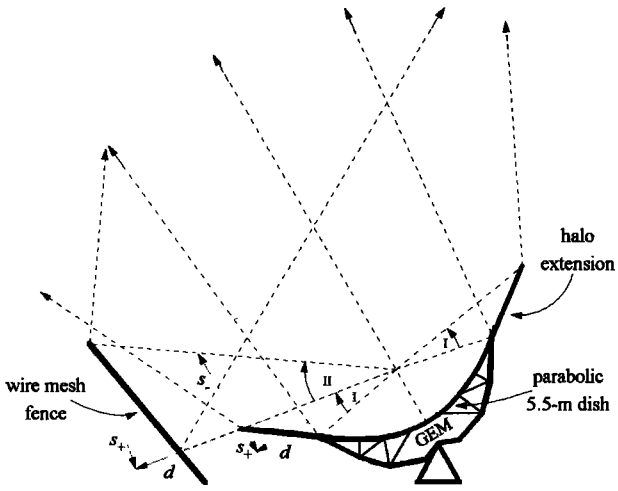

Figure 1. Side view of the instrument showing a ray-tracing diagram (dashed lines) for the reflector and the shields. Sidelobes into region I will fall upon the halo and pick up the sky instead of the ground, while the fence causes partial reflection of the sky signal and partial transmission of the ground signal into the sidelobes of region II. The projections s and d are used in the Fresnel method of diffraction to represent full range in aperture distance from the diffracting edge and distance to the assumed aperture plane, respectively.

2. Experimental Design

The GEM antenna consists of a portable 5.5-m radio telescope with an extension halo made of 2.1-m-long aluminum sheet panels. The instrument mount is an altazimuth rotating base for circularly scanning the sky around the zenith at 1 rpm. The daily rotation of the Earth spreads out the scans to map a full declination band in the sky. The experiment was designed so that the halo would intercept much of the solid angle in the direction of the ground, thereby redirecting the spillover sidelobes toward the sky. However, in order to minimize the response from the diffraction sidelobes which see the edges of the halo (a problem that worsens with increasing wavelength), a ground screen, or fence of hexagonal wire mesh, was erected around the radio telescope (Figure 1). In addition, this outer shield should act as an effective means for leveling out at the prime focus the increased proportion of ground seen above the lower edge of the tilted dish.

Kraus coils in the backfire mode were developed as feeds for a prime focus arrangement at 408 and 1465 MHz [*De Amici*, 1995]. Conventionally speaking, a Kraus coil is made of a helical conductor rising above a ground plane near the feed point, and the radiation mode is determined by the relative size of the ground plane. If the diameter of the ground plane is made less than the diameter of the helix, the excited waves are launched backward in the direction of the feed point (backfire mode); whereas if the diameter of the ground plane is larger than twice the diameter of the helix, the waves are launched from the open end of the helix (end-fire mode). The advantages of backfire antennas as feeds for a relatively small sized 5.5-m dish are considerable: (1) reduced aperture blockage and (2)

sensitivity to circular polarization. The latter becomes important because galactic radio emission is dominated by intrinsically polarized synchrotron radiation at these wavelengths. Unlike dipoles and horns, helical feeds use coaxial cables for transmission lines and avoid unnecessary system noise due to the absence of coaxial adapters and/or orthomode transducers for total intensity measurements. Besides, in the backfire mode the length of the coaxial cable can be made conveniently short to minimize line losses. Table 1 summarizes the geometrical characteristics of our feeds.

In view of the analytical approach intended in this paper and the difficulty in assessing the theoretical aspects of the radiation pattern in the backfire mode [*De Amici*, 1995, and references therein], we use in our calculations of the primary the far-field pattern (its normalized electric field) for monofilar axial-mode helical antennas [*Kraus*, 1988]:

$$E_n = \sin\left(\frac{90°}{n}\right)\frac{\sin(n\psi/2)}{\sin(\psi/2)}\cos\theta\,, \qquad (1)$$

where the phase difference $\psi = 360°[S_\lambda(1 - \cos\theta) + 1/2n]$ is given for increased-directivity condition, θ is the backfire polar angle, and n (= 9.5 for our feeds) is the number of loops spaced at regular intervals of S_λ units (see Table 1). Despite our inadequacy to supply, at this stage, a more realistic functional expression for the backfire mode of our feeds, the axial-mode prime feed pattern we have chosen displays low-level spillover and diffraction sidelobes in the halo region (see Figure 2), as required by our experiment.

Table 1. Backfire Helices of the Galactic Emission Mapping Project

Frequency,	λ,	Free-Space Wavelengths			α,[d]
MHz	cm	C_λ[a]	S_λ[b]	ρ_λ[c]	deg
408	73.48	0.919	0.209	0.013	12.8
1465	20.39	0.990	0.215	0.023	12.3

[a]The length of the circumference of each loop.
[b]The spacing between neighboring loops.
[c]The diameter of the helical conductor.
[d]The pitch angle $\alpha = \arctan(S_\lambda/C_\lambda)$.

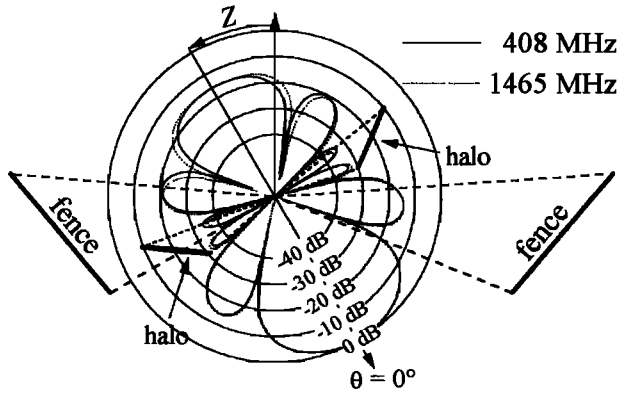

Figure 2. Side view of the shields superposed on the polar diagrams of the monofilar axial-mode patterns used in our calculations of the prime feed response at 408 MHz (dashed lines) and 1465 MHz (dotted lines). The tilt angle Z is 30°.

3. Ground Emission

The presence of the shields modifies the response of the feed in the direction of the sidelobes exposed to ground radiation. We evaluate this effect by using the geometric theory of diffraction, which makes a clear distinction as to the treatment of such phenomena in terms of the separation of the source of radiation (the ground), the physical obstruction responsible for the diffraction (the shields), and the location where the variation of the source intensity is verified (the feed).

When the phenomena become independent of the distance to the source, the variation of its intensity exemplifies the well-known Fraunhofer diffraction pattern, or far-field pattern. If the phenomena under investigation, on the other hand, depend on the distance, the result is a Fresnel, or near-field, diffraction pattern. Thus the modification of the feed response is seen as the effect of the diffraction pattern of the shields on the diffraction pattern of the feed.

For either pattern, the threshold between the two regimes is usually given in terms of the distance $d_r \approx 2a_l^2/\lambda$, where a_l is the linear dimen-

sion of the aperture associated with the diffracting obstruction. In the case of the shields, we shall assume that the obstructions are effectively represented by the upper edge of the fence and the outer edge of the halo. The corresponding aperture can be given, approximately, by the height of a diffraction slit with a linear dimension of 1λ. The implied thresholds lie at $\sim$1.5 m at 408 MHz and at $\sim$0.5 m at 1465 MHz. For the feed, however, the linear dimension of its aperture has been estimated from the square root of its effective area (λ^2 / feed solid angle). So $d_r(408\,\mathrm{MHz}) \approx 2.75\,\mathrm{m}$ and $d_r(1465\,\mathrm{MHz}) \approx 0.77\,\mathrm{m}$, which places the edges of the shields immediately outside the near-field zone of the feed pattern.

Analytically, the rather close proximity of the deduced thresholds between the diffraction patterns of the feed and the shields (of the halo, in particular) poses an interesting problem as to their mutual coupling in practice. Although we do expect our estimates of the diffraction effects to represent a distance dependent Fresnel regime, we also would like to know how significantly different this approach could be when compared with a distance independent Fraunhofer approximation. Therefore we will start by making the simplifying assumption that the bulk of the emission from the ground arrives at the fence in the form of parallel wave fronts (source at infinity) and estimate the diffraction effects with the Fraunhofer formalism. Then, we will make the more precise assumption that the blockage of the ground by the shields produces a Fresnel diffraction pattern. The analytical tools are given in sections 3.1-3.3, while the estimates from both approaches are compared in section 4.

3.1. The Transmitted Component

The relative importance of the diffracted radiation at the fence and, consequently, the transmitted power diffracted at the portion of the halo hidden by the fence are directly related to the attenuation properties of the wire mesh screen. In order to model the fence we simplify the mesh treatment to a superposition of two mutually orthogonal sets of parallel wires. *Mumford* [1961, and references therein] improved on existing attenuation formulae to account for the experimental results quoted by other authors and assembled an empirical nomograph for the case of plane waves arriving at an arrangement of parallel wires of diameter $2r$ and separated by a spacing a, such that the ratio κ of the transmitted to the incident power, P_t/P_i, is given by

$$\kappa \equiv \frac{P_t}{P_i} = \left(\frac{\Lambda}{2}\right)^{-2} \tag{2}$$

with

$$\Lambda(\lambda, r, a) = \lambda_a \left[\ln\left(\frac{0.83 \exp C_a}{\exp C_a - 1}\right)\right]^{-1}, \tag{3}$$

where λ_a is the wavelength and $C_a \equiv 2\pi r/a$ is the circumference of the wire in units of the spacing a. This is the case for normal incidence and linearly polarized waves in the direction perpendicular to the orientation of the wires. In the more general situation of unpolarized radiation arriving at an angle φ to the fence, the incident power may be decomposed as the sum of two equal and independent contributions. One will originate a transmitted component in the fashion outlined by (2), whereas the other will yield a component just like in (2) but with an effective spacing scaled by $\sin\varphi$. Thus the overall attenuation becomes

$$\kappa = 2\left[\Lambda^{-2}(\lambda, r, a) + \Lambda^{-2}(\lambda, r, a\sin\varphi)\right]. \tag{4}$$

Figure 3 shows the effect of conductor diameter and spacing on the attenuation coefficient κ for the working frequencies in our mapping experiment. As meant by our design considerations, the open circle in Figure 3 indicates that the present fence ($a = 5\,\mathrm{cm}$, $r = 0.5\,\mathrm{mm}$, and $\varphi = 50°$) should provide a reasonable level of attenuation ($\sim$10 dB) at our lowest frequency.

For a fence that levels out at the prime focus of the paraboloid, the increased proportion of ground seen in front of the tilted dish, the transmitted power will contribute to the antenna temperature through the solid angle of region II (halo present) or of regions I and II (halo absent) in Figure 1. The total ground solid angle

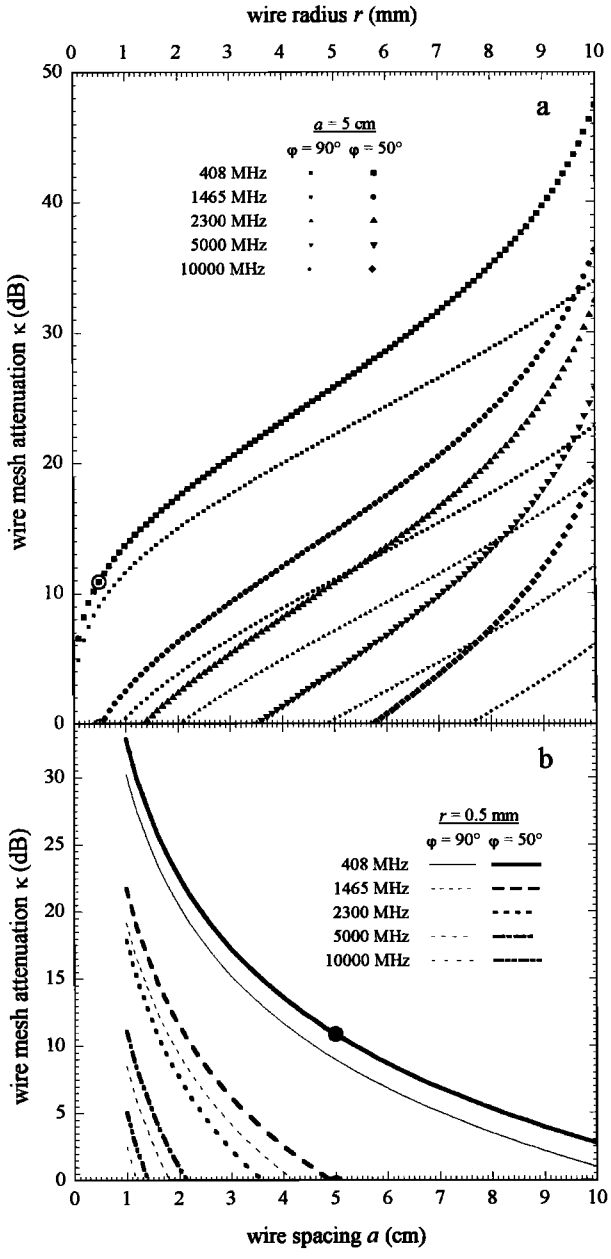

Figure 3. Expected wire mesh screening of the fence as (a) a function of wire radius r and spacing of 5 cm and (b) a function of spacing a for 1-mm-diameter wires. The full circles indicate the expected attenuation at 408 MHz.

is bounded above by the edge of the fence at $\theta_{f_\phi} \equiv \theta_f(\phi)$ and below by the edge of the halo at θ_h, such that the transmitted antenna temperature component will amount to

$$T_{A,\oplus}^{\mathrm{tr}} \approx \bar{T}_\oplus \frac{1}{\Omega_A} \int_{\phi_c}^{2\pi-\phi_c} \int_{\theta_h}^{\theta_{f_\phi}} \kappa(\theta) E_n^2(\theta)\, d\Omega\,, \quad (5)$$

where ϕ_c is the azimuth at which the line of sight to the edge of the halo intercepts the edge of the fence ($\theta_h = \theta_{f_\phi}$), Ω_A is the solid angle of the feed, and $\bar{T}_\oplus$ is an average physical temperature of the ground.

3.2. The Diffracted Components in the Fraunhofer Regime

The diffraction of plane waves by a slit of height y and width x will produce a variation in the intensity of the radiation at a point Q given by [*Jenkins and Harvey*, 1981]

$$I \propto \frac{\sin^2 \beta_y}{\beta_y^2} \times \frac{\sin^2 \gamma_x}{\gamma_x^2}\,, \quad (6)$$

where $\beta_y \equiv (\pi y/\lambda) \sin\theta_y$, $\gamma_x \equiv (\pi x/\lambda) \sin\phi_x$ and θ_y and ϕ_x specify the direction of Q from the center of the slit. For the circular arrangement of the wire mesh screens of the fence and of the sheet metal panels of the halo, a collection of diffraction slits along their edges may be thought of as an overall annular slit. (These edges do not conform to strictly circular shapes. Those of the halo make up a regular polygon of 24 sides, while the ones of the fence assemble into a dodecagon. The annular approximation is justified in view of the relatively long wavelengths under consideration.) In the limit of infinitesimally wide slits and the location of Q at the prime focus of the paraboloid, the deviation in azimuth from $\phi_x = 0°$ is small compared with the range in θ_y, so that the diffracted component of the ground contribution to the antenna temperature can be approximated by

$$\begin{aligned} T_{A,\oplus}^{\mathrm{df}} = \frac{\bar{T}_\oplus}{\Omega_A} \Bigg\{ & \int_{\phi_c}^{2\pi-\phi_c} \Bigg[\int_{\theta_h}^{\theta_{h+\lambda}} \frac{\sin^2 \beta_y}{\beta_y^2} \kappa(\theta)\, dF_\theta \\ & + \int_{\theta_{f_\phi}}^{\theta_{f_\phi+\lambda}} \frac{\sin^2 \beta_y}{\beta_y^2} [1 - \bar{\kappa}(\theta)]\, dF_\theta \Bigg] d\phi \\ & + \int_{-\phi_c}^{\phi_c} \int_{\theta_h}^{\theta_{h+\lambda}} \frac{\sin^2 \beta_y}{\beta_y^2} E_n^2(\theta)\, d\Omega \Bigg\} \end{aligned} \quad (7)$$

where $\bar{\kappa}(\theta)$ corresponds to the mean attenuation from θ_h to θ_{f_ϕ} and $dF_\theta \equiv E_n^2(\theta)\sin\theta\, d\theta$. Note that the contribution due to the halo is separated into two parts. The second integral inside the brackets accounts for the diffraction of the component transmitted by the fence, while the integral outside of them refers to the diffraction of direct ground pickup at the portion of the halo that looms above the fence.

3.3. The Diffracted Components in the Fresnel Regime

A more precise approach to the antenna temperature contribution from the ground can be investigated if we apply the well-known optical analysis of Fresnel diffraction by a straight edge to our double-shielded antenna configuration. Thereby we extend the notion of plane waves arriving in the aperture planes of the shields to a distance dependent source. For such, let Ω_f be the solid angle that the fence profile fills out from the prime focus of the paraboloid. Then, if (1) we treat the ground source as a uniform temperature distribution over Ω_f, (2) we choose the aperture plane of the fence to lie perpendicular to the line of sight that clears the edge of the halo, and (3) we choose the aperture plane of the halo to lie perpendicular to the line of sight that bounds Ω_f from below, an estimate of the ground contribution to the antenna temperature is readily obtained by convolving the ground temperature distribution with a modified feed response according to [*Kraus*, 1966],

$$T_{A,\oplus} = \frac{\bar{T}_\oplus}{\Omega_A}\iint_{\Omega_f} P[qs(\theta_h-\theta)]\kappa(\theta)E_n^2(\theta)\,d\Omega + \frac{\bar{T}_\oplus}{\Omega_A}\int_{\phi_c}^{2\pi-\phi_c}\int_{\theta_h}^{\theta_{f_\phi}} P[qs(\theta_{f_\phi}-\theta)] \times [1-\kappa(\theta)]E_n^2(\theta)\,d\Omega\,, \quad (8)$$

where $P(qs)$ is the relative power response of the feed as given by

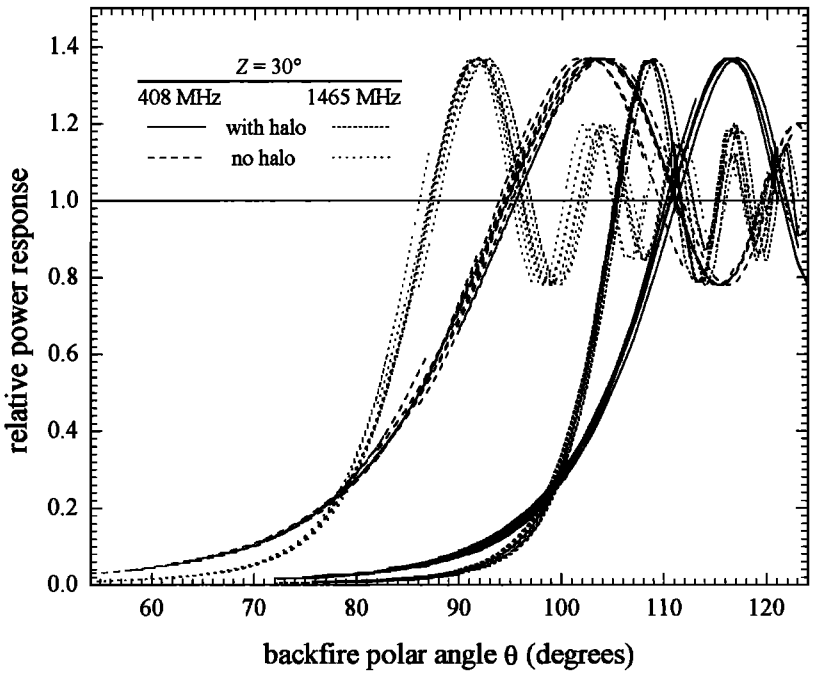

Figure 4. Profiles of the relative power response of the feed for the dish with and without the halo and sampled at 10° intervals in the azimuth range $\phi_c \le \phi \le 2\pi - \phi_c$. The tilt angle Z is 30°.

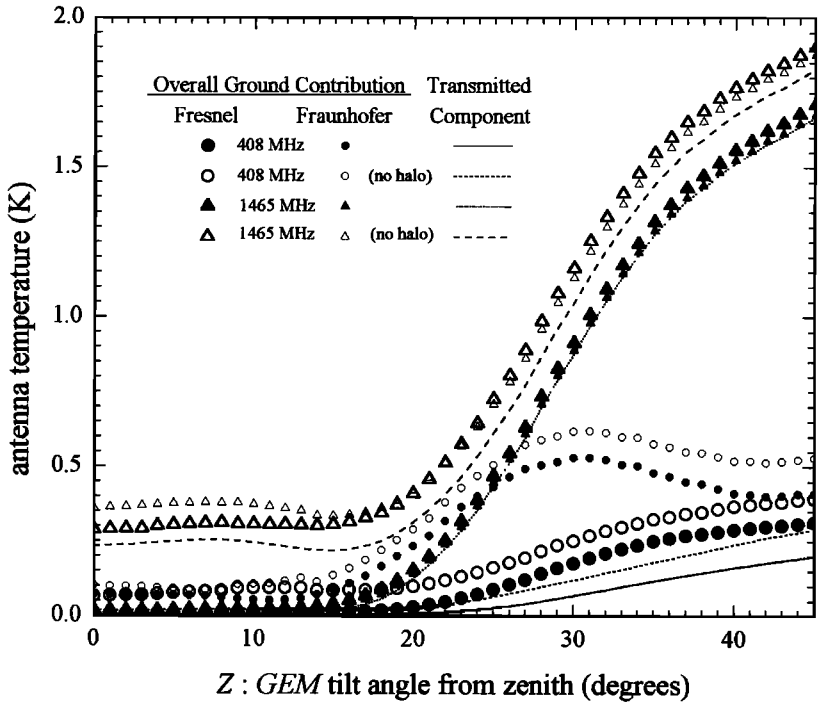

Figure 5. Total and transmitted component of the antenna temperature contribution due to ground emission for the dish with the halo on (solid symbols) and for the dish alone (open symbols).

$$P(qs) = \frac{1}{2}\left\{\left[\frac{1}{2} - C(qs)\right]^2 + \left[\frac{1}{2} - S(qs)\right]^2\right\} \quad (9)$$

and qs models the geometry of the blockage in terms of the distance $d(= 2/q^2\lambda)$ to the aperture plane and the aperture distance s from the diffracting edge (see Figure 1). In 9 the quantities $C(qs)$ and $S(qs)$ are the cosine and sine Fresnel integrals:

$$C(qs) = \int_0^{qs} \cos\left(\frac{\pi u^2}{2}\right) du \quad \text{and} \quad (10)$$

$$S(qs) = \int_0^{qs} \sin\left(\frac{\pi u^2}{2}\right) du\,, \quad (11)$$

with $u = qx$ for $0 \leq x \leq s$. Figure 4 illustrates the amount of distortion the feed response is subject to, as the halo partially blocks the inner aperture plane in the exposed region of the fence ($\phi_c \leq \phi \leq 2\pi - \phi_c$). Still, in (8) it should be noted that the first term of the convolution integral includes the transmitted component given by (5), which has to be subtracted to obtain the diffraction component due to the entire halo alone. The second term in (8) makes up for the diffracted component by the fence.

4. Results and Discussion

Our estimates of the overall ground contribution to the antenna noise temperature cover the allowed instrumental range of $0 \leq Z \lesssim 45°$ at 1° steps from zenith and are shown in Figure 5. The displayed calculations include, in addition to the difference in obtaining diffraction estimates with the Fraunhofer and Fresnel methods, the effect of removing the halo. Also shown are the sole contributions from the component transmitted through the fence and, at large tilt angles, picked up directly from unscreened ground below the fence (see Figure 6).

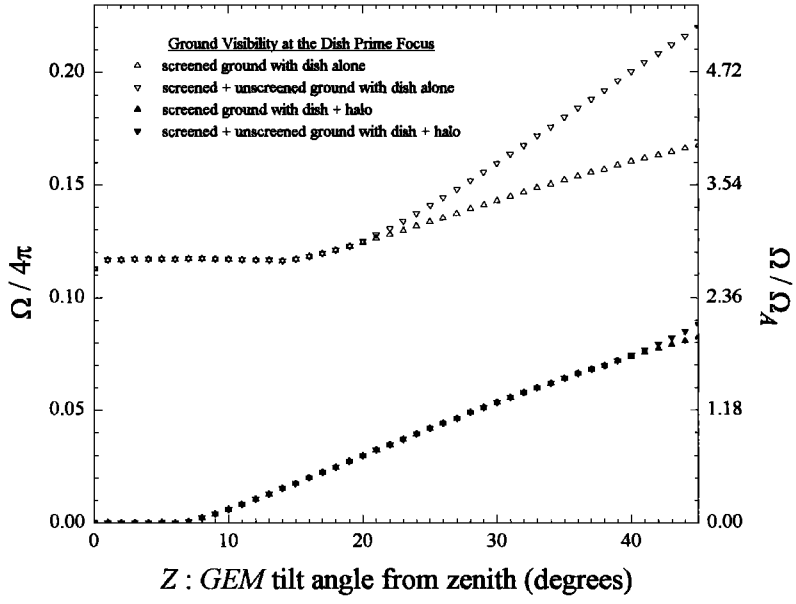

Figure 6. The solid angle fraction filling out the ground seen between the upper edge of the fence and the rim of the halo (solid symbols) or the dish (open symbols). Unscreened portions are revealed when the line of sight to the rim of the halo drops below the lower edge of the fence.

Because ground shielding acts directly on the bulk of the radiation, we see immediately how crucially important efficient screening can be in keeping the ground contribution at a low level. In this case, the diffracted components can dominate the overall contribution for tilt angles $Z \lesssim 35°$ (halo on) and $Z \lesssim 30°$ (halo off). In order to better understand the specific role of the shields in this context, though, we shall separate their diffracted components as described below.

Figure 7 compares the effect of efficient screening on the level of the diffracted component of the fence. At 408 MHz, where the screening is significant, the level of the sidelobes in the direction of the halo is low enough to make diffraction effects at the fence insensitive to the presence of the halo for $Z \gtrsim 25°$. At lower angles ($Z \lesssim 25°$), fence visibility (see Figure 8), rather than low sidelobes, brings up distinct contributions for the dish with and without halo.

Also, since the attenuation of the fence is already low at 1465 MHz, not even changes in fence visibility should affect the diffraction at the fence. Figure 7 shows that the Fresnel approach is consistent with this expectation, but the Fraunhofer approximation only agrees for $Z \gtrsim 30°$, when the halo-independent condition is more likely to apply due to low sidelobe level.

If we take the case at 408 MHz to be representative of the diffraction by the fence, then Figure 7 tells us that the Fraunhofer approximation overestimates the results of the Fresnel approach. Their discrepancy gets worse in the interval $15° \lesssim Z \lesssim 25°$, where the estimates differ by a full order of magnitude (~10 dB), but improves steadily down to the 3-dB level toward the largest tilt angles. Diffraction at the rim of the halo or dish, on the other hand, shows according to Figure 9 that eventually, Fraunhofer and Fresnel estimates will reach equal noise levels at some tilt angle we have denoted as Z_{eq}. With the exception of the diffraction at the edge of the dish in the 408-MHz case, the Fraunhofer approximation underestimates the Fresnel calculations for tilt angles $Z > Z_{eq}$.

If we now express the distance of these diffract-

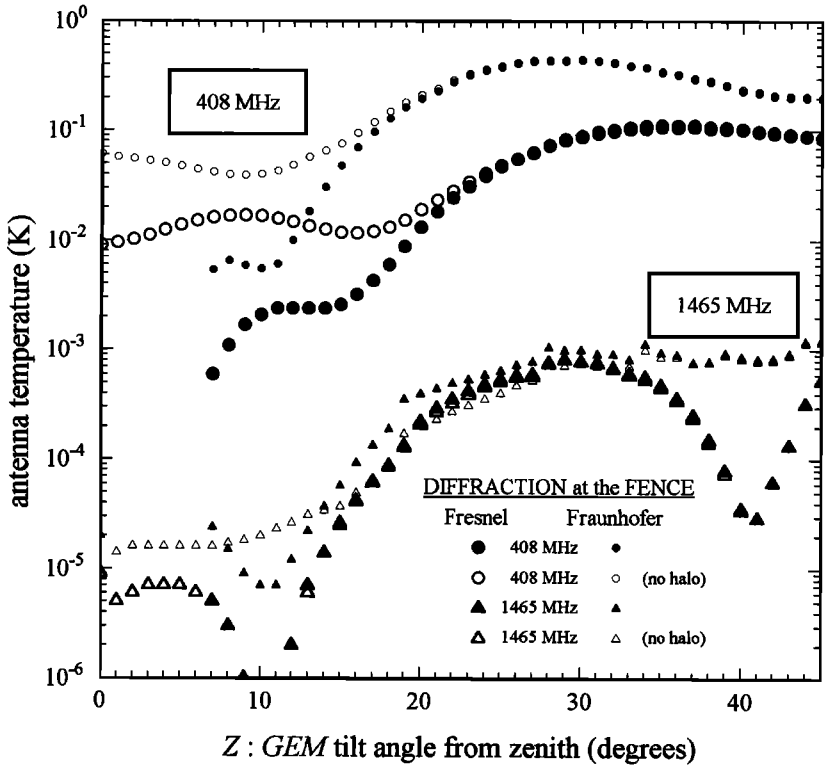

Figure 7. Antenna temperature contribution due to diffraction of ground radiation at the upper edge of the fence. Solid symbols indicate dish with halo; open symbols indicate dish without halo.

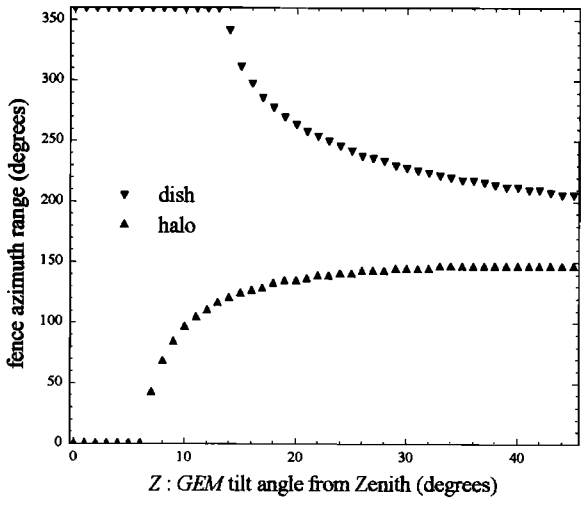

Figure 8. Fence visibility at the prime focus expressed as the angular extent of the upper edge of the fence between ϕ_c and $2\pi - \phi_c$.

ing edges from the prime focus in units of the threshold distance to the near-/far-field boundary of the feed pattern, then, as summarized in Table 2, the above behavior argues in favour of a distance dependent effect.

Thus, as Z_{eq} increases in cases A-C, the diffracting edges will appear closer to the feed threshold. In case D, the Fresnel diffraction patterns of the feed and of the dish edge may already be overlapping considerably. Still, when comparing the estimates by size between those at small and large tilt angles, there is again a good 10-dB difference when the halo is present, but only some 5 dB when it is removed.

The relative importance of the shields in contributing through their diffracted components to the antenna noise temperature can be obtained by comparing Figures 7 and 9. Keeping

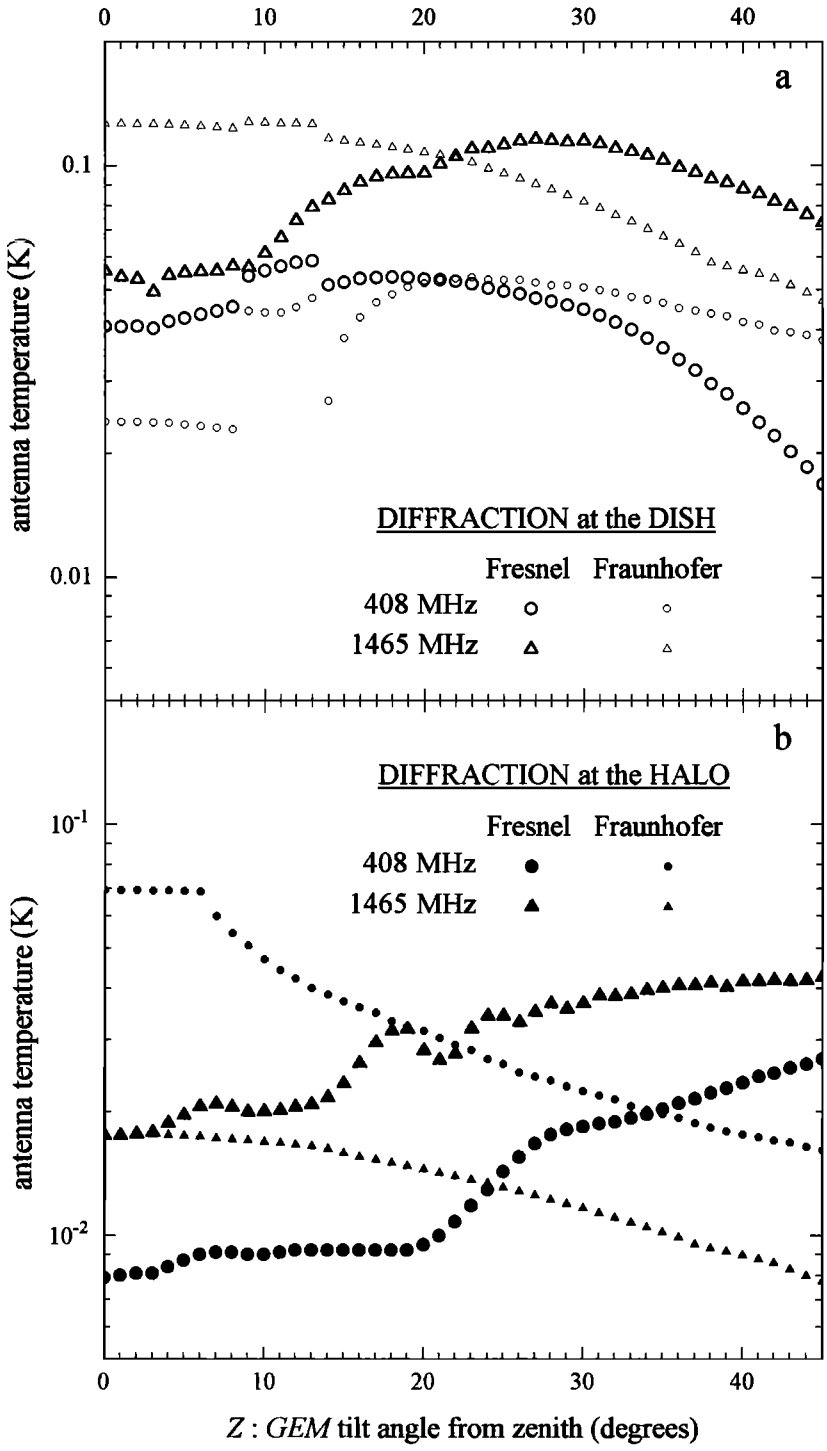

Figure 9. Antenna temperature contribution due to diffraction of ground radiation at the outer edges of the halo (solid symbols) and of the dish (open symbols) as a function of tilt angle in the GEM experiment at (a) 408 MHz and (b) 1465 MHz.

Table 2. Equivalence Between Fraunhofer and Fresnel Diffraction Estimates

Case	Diffracting Edge	Location d_r units[a]	Z_{eq}, deg
A	halo at 1465 MHz	5.8	< 5
B	dish at 1465 MHz	3.6	22
C	halo at 408 MHz	1.6	35
D	dish at 408 MHz	1.0	21

[a]Here $d_r \approx 2\lambda\,\Omega_A{}^{-1/2}$.

the discussion this time to the estimates in the Fresnel regime, we verify that with the efficient screening at 408 MHz the fence dominates the diffraction effects for $Z \gtrsim 20°$. An extreme is reached around $Z \approx 30°$-$35°$, when the diffraction at the fence is about 7 dB noisier than at the halo. If the halo is absent, however, the fence will dominate only in the halo-independent region ($Z \gtrsim 25°$), while still attaining a 7-dB difference at the largest tilt angles. Despite the lack of efficient screening at 1465 MHz, which makes the halo at least 16 dB noisier than the fence for tilt angles near $Z \approx 30°$, the absence of the halo would contribute with an additional 5 dB to this relative noise level. From Figure 5, however, we know that even so, the diffracted components here are some 14 dB below the noise due to transmission alone.

5. Summary and Conclusions

We have developed a model for a double-shielded antenna to estimate the transmitted and diffracted components of the radiation emitted by the ground. We apply the geometrical methods of Fraunhofer and Fresnel diffraction to test the performance of the antenna as a function of antenna tilt angle Z (from zenith) in the range $0° \geq Z \geq 45°$ against screening efficiency of an outer shield (a fence) and removal of an inner shield (a halo). Definite predictions were found for a Kraus coil as feeder for the radiometric system.

By requiring a low response of the feed sidelobes that illuminate the halo, we find evidence that diffraction will contribute more than transmission to the antenna noise temperature as long as the screening efficiency of the fence is significant (~10 dB). This condition is realized in the Fraunhofer regime for all tilt angles, but in the Fresnel regime it is tilt angle limited ($Z \lesssim 35°$ with halo and $Z \lesssim 30°$ without halo). Similarly, whereas in the Fraunhofer regime the diffraction component is dominated by the fence (except for $Z \lesssim 15°$ when the halo is on), in the Fresnel regime the contribution of the halo/dish becomes more relevant and exceeds that of the fence for $Z \lesssim 20°$ (halo on) and for $Z \lesssim 25°$ (halo off). For tilt angles $Z \gtrsim 25°$ the contribution of the fence not only makes up for most of the diffracted component but also becomes independent of the presence of the halo in either regime. If screening is inefficient (<1 dB), transmission becomes dominant and reflects directly the increased proportion of ground seen in front of the antenna with tilt angle.

We also conclude that there is a correlation between tilt angle and the proximity of the diffracting edge of the halo from the near-/far-field boundary of the feed pattern, such that as long as there is no significant coupling between the near-field patterns of both the feed and the diffracting halo, estimates using the Fraunhofer approximation agree with those calculated with the Fresnel approach at a tilt angle Z_{eq}. In these cases, the Fraunhofer method will produce estimates that are higher than those obtained with the Fresnel method for $Z \lesssim Z_{eq}$ and lower for $Z \gtrsim Z_{eq}$. The higher estimates in the Fraunhofer regime are also found for the fence, as expected for a location in a region still farther away from the near-/far-field boundary.

Acknowledgments. We thank Michele Limon, Chris Witebsky, John Yamada, and Doug Heine for their valuable contributions during the development of the GEM hardware. Two of us, C. Tello and T. Villela, thank FAPESP for supporting the GEM project in Brazil under proccess numbers 97/03861-2 and 97/06794-4. M. Bersanelli acknowledges the support of the NATO Collaborative Grant CRG960175.

References

Davies, R. D., R. A. Watson, and C. M. Gutiérrez, Galactic synchrotron emission at high frequencies, *Mon. Not. R. Astron. Soc., 278,* 925-939, 1996.

De Amici, G., S. Torres, M. Bensadoun, M. Bersanelli, G. Dall'Oglio, M. Limon, G. Smoot, T. Villela, and C. Witebsky, A research program to map the galactic emission at low frequencies, *Astrophys. Space Sci., 214,* 151-158, 1994.

De Amici, G., The 408 MHz beam antenna profile, *Astrophys. Note 482,* 7 pp., Space Sci. Lab., University of California, Berkeley, 1995.

Haslam, C. G. T., C. J. Salter, H. Stoffel, and W. E. Wilson, A 408 MHz all-sky continuum survey, II, The atlas of contour maps, *Astron. Astrophys. Suppl. Ser., 47,* 1-143, 1982.

Jenkins, F. A., and W. E. Harvey, Diffraction, in *Fundamentals of Optics,* 4th ed., pp. 315-334, McGraw-Hill, New York, 1981.

Kogut, A., A. J. Banday, C. L. Bennett, K. M. Gorski, G. Hinshaw, and W. T. Reach, High-latitude galactic emission in the COBE DMR two-year sky maps, *Astrophys. J., 460,* 1-9, 1996a.

Kogut, A., A. J. Banday, C. L. Bennett, K. M. Gorski, G. Hinshaw, G. F. Smoot, and E. L. Wright, Microwave emission at high galactic latitudes in the four-year DMR sky maps, *Astrophys. J., 464,* L5-L19, 1996b.

Kraus, J. D., *Radioastronomy,* 481 pp., McGraw-Hill, New York, 1966.

Kraus, J.D., *Antennas,* 2nd ed., 892 pp., McGraw-Hill, New York, 1988.

Lawson, K. D., C. J. Mayer, J. L. Osborne, and M. L. Parkinson, Variations in the spectral index of the galactic radio continuum emission in the northern hemisphere, *Mon. Not. R. Astron. Soc., 225,* 307-327, 1987.

Mumford, W. W., Some technical aspects of microwave radiation hazards, *Proc. IRE, 49*(2), 427-447, 1961.

Platania, P., M. Bensadoun, M. Bersanelli, G. De Amici, A. Kogut, S. Levin, D. Maino, and G. F. Smoot, A determination of the spectral index of galactic synchrotron emission in the 1-10 GHz range, *Astrophys. J., 505,* 473-483, 1998.

Reich, P., and W. Reich, A radio continuum survey of the northern sky at 1420 MHz, II, *Astron. Astrophys. Suppl. Ser., 63,* 205-292, 1986.

Reich, P., and W. Reich, A map of spectral indices of the galactic radio continuum emission between 408 MHz and 1420 MHz for the entire northern sky, *Astron. Astrophys. Suppl. Ser, 74,* 7-23, 1988.

Tello, C., An experiment to measure the total sky brightness at centimeter-long wavelengths, Ph.D. thesis, 174 pp., Inst. Nac. de Pesq. Espaciais, São José dos Campos, São Paulo, Brazil, August 1997.

Torres, S., et al., The GEM project: An international collaboration to survey galactic radiation emission, *Astrophys. Space Sci., 240,* 225-234, 1996.

M. Bensadoun and G. F. Smoot, Lawrence Berkeley National Laboratory, University of California at Berkeley, 1 Cyclotron Road, Building 50, MS 205, Berkeley, CA 94720. (e-mail: bensadoun@galaxy.lbl.gov; smoot@galaxy.lbl.gov)

M. Bersanelli, Istituto di Fisica Cosmica, Consiglio Nazionale delle Ricerche, Via Bassini 15, 20133 Milano, Italy. (e-mail: marco@ifctr.mi.cnr.it)

G. De Amici, TRW R1/2128, 1 Space Park Drive, Redondo Beach, CA 90278. (e-mail: g.deamici@trw.com)

N. Figueiredo, Escola Federal de Engenharia de Itajubá, Av. Benedito Pereira dos Santos 1303, Itajubá, Minas Gerais 37500-000, Brazil. (e-mail: newton@cpd.efei.br)

C. Tello, T. Villela, and C. A. Wuensche, Divisão de Astrofísica, Instituto Nacional de Pesquisas Espaciais, CP 515, São José dos Campos, São Paulo 12201-970, Brazil. (e-mail: tello@das.inpe.br; villela@das.inpe.br; alex@das.inpe.br)

S. Torres, Observatorio Astronómico, Universidad Nacional de Colombia and Centro Internacional de Física, Bogotá, Colombia. (e-mail: storres@earthlink.net)

(Received April 1, 1998; revised October 20, 1998; accepted November 27, 1998.)